Block Copolymer Micelles in Dilute Solution

Tadao Kotaka,*[1a] Takeshi Tanaka,[1b] Mitsuhiro Hattori,[1b] and Hiroshi Inagaki[1b]

Department of Polymer Science, Osaka University, Toyonaka, Osaka 560, and Institute for Chemical Research, Kyoto University, Uji, Kyoto 611, Japan. *Received August 12, 1977*

ABSTRACT: A light-scattering study was carried out to examine the micelle-forming behavior of polystyrene (PS) and poly(methyl methacrylate) (PMMA) block copolymers of SM-diblock and MSM-triblock types in toluene (TOL)-/*p*-cymene (pCY) mixture. Both solvents are (nearly) isorefractive to PMMA and good solvents to PS, but pCY is a nonsolvent to PMMA. Upon increasing pCY content, micelles are formed through the aggregation of (nearly invisible) PMMA blocks. Their morphologies are different depending on pCY content, the type of block copolymers involved, etc. In SM-diblock copolymer systems with intermediate pCY content, spherical-shape micelles with a PMMA core, and PS fringes appear to be formed. A theoretical particle scattering function was derived for such a spherical micelle model and compared with the experiments: The fringe PS chains appear to be considerably expanded as compared with the equivalent precursor PS chains, and a substantial extent of PS–PMMA intermixing must have been taking place. At higher pCY content regions, more extended ellipsoidal or cylindrical-shape micelles appear to be present. On the other hand, an MSM-triblock system exhibits in the light-scattering Zimm plot rectilinear scattering envelopes, which suggests the existence of network-like or highly branched-type micelles through the successive aggregation of two PMMA side blocks in the molecules.

Because of the mutual incompatibility of two different homopolymers, the constituent blocks of a block copolymer usually undergo microphase separation in bulk and in concentrated solution. The phenomenon is important even in dilute solution, especially of selective solvents, resulting in the formation of stable micelles.[2-4] The object of this paper is to examine the micelle-forming behavior of AB-diblock and BAB-triblock copolymers mainly by using classical Rayleigh scattering method. In this light-scattering study we adopted an approach suggested by Leng and Benoit[5,6] and also by Utiyama and Kurata,[7,8] i.e., to utilize isorefractive solvent which has nearly zero refractive index increment for either one of the constituent homopolymers. However, one should be careful in such analyses, since the measurements are usually made with solvents in which, say, the B block is still slightly visible. As we pointed out before,[9] even a small visibility amounts to an unexpectedly large contribution, especially when the slightly visible B block is highly expanded in comparison with the fully visible A block. In this study we also have examined this aspect.

In previous articles[3,4] we dealt with a similar problem. There we examined the behavior of polystyrene (PS) and poly(methyl methacrylate) (PMMA) block copolymers of SM and MSM types in several solvent systems having different solubility to PS and PMMA. We found most striking contrast between their behavior in selective solvents of the type which is poor for PMMA but is good for PS. Particularly in *p*-xylene, an MSM-block copolymer appeared to undergo intrachain association between the two PMMA side blocks, thereby resulting in the formation of unimolecular micelle.

An interesting report on the micelle-forming behavior of AB-diblock copolymer was published also by Kurata et al.,[8] who examined a PS–PMMA diblock copolymer in toluene (TOL) and furfuryl alcohol (FAL) mixture. Both solvents are nearly isorefractive to PMMA, and TOL is a good solvent for both PS and PMMA, while FAL is a nonsolvent for PS and a good solvent for PMMA. Therefore, upon increasing FAL content in the mixture the block copolymer molecules tend to form micelles through the aggregation of visible PS blocks.

In this article we will report some results of light-scattering studies on PS and PMMA block copolymers of SM and MSM types in TOL and *p*-cymene (pCY) mixture, placing emphasis on the contrast between their behavior. Here both solvents are nearly isorefractive to PMMA. However, the TOL/pCY mixture has the selectivity opposite to the TOL/FAL mixture, i.e., pCY is a nonsolvent for PMMA but a good solvent for PS. The block copolymer molecules would form micelles through the aggregation of invisible PMMA blocks, and there should be a contrasting difference between the behavior of the SM- and MSM-block copolymers. In addition, we will attempt to interpret some of these light-scattering data from SM-diblock copolymer solutions (in which we expect the block copolymer molecules to form micelles of certain simple morphology), introducing a model compatible with such micelles.

Experimental Section

Materials. An MSM-triblock sample and three SM-diblock samples of PS and PMMA and PS precursors were prepared by an anionic polymerization technique as described before.[11,12] The three SM-diblock samples have the same PS precursor as the S block and PMMA blocks of different lengths as the M blocks. All these polymer samples were characterized according to our laboratory routine, which was described elsewhere.[3,11,12] Here we only list the results in Table I. The solvents were TOL and pCY, of which the refractive index increments for PS and PMMA are listed in Table II.

Methods. Light-scattering measurements were made on a Fica light-scattering photometer Model 50. Again the details were described elsehwere[12] and will not be recounted here. However, we wish to remark that the optical cleaning of solutions of the mixed solvent with high pCY content was often difficult by our routine centrifugation procedure[12] obviously because of the micelle formation. Therefore, we employed the following procedure for this purpose.[13] First we dissolved an adequate amount of a block copolymer sample in fractionally distilled benzene. The benzene solution was then centriguged for 150 min at 24 000 rpm in a Hitachi preparative centrifuge Model 55P in a fixed-angle rotor RP30. The central portion of the cleaned solution was carefully transferred to a light-scattering cell with a ground glass stopper. Then benzene was thoroughly removed by freeze–drying in the cell. Solvents, TOL and pCY, were separately purified first by fractional distillation followed by centrifugation for 150 min at 27 000 rpm. The purified solvents were mixed to a desired composition. Then a prescribed amount of the mixture was introduced into the light-scattering cell, in which the previously deposited polymer was dissolved at an elevated temperature (about 60 °C whenever necessary) to yield a final solution. The polymer concentration was determined by weighing the whole cell before and after the dilution. The solutions especially of high pCY content were slightly opaque. Even so, they were stable and did not show any time-dependent changes of the scattered light intensities. The results were reproducible and independent of a particular process employed for the sample preparation (e.g., thermal history, etc.). All the measurements were made at 30.0 ± 0.3 °C. Vertically polarized light (V_v component) was observed at 13 different angles between 15 and 150° using vertically polarized incident light of 436-nm wavelength. (In a few cases we also used 546-nm light.) Occasionally measurements of horizontally polarized (H_v) component were made to test the influence of the optical anisotropy, if any were present, upon micelle formation. The anisotropy was found negligibly small in all cases.

0024-9297/78/2211-0138$01.00/0

Table I
Characteristics of Polystyrene–Poly(methyl methacrylate) Block Copolymer Samples

Code	Type	ST content x_A	$10^{-4}M_w$	M_w/M_n
63B30	PS–PMMA	0.24	150 ± 10	
63B50	PS–PMMA	0.49	76.4	1.13
63B70	PS–PMMA	0.69	64 ± 5	
63H	Precursor PS	1.00	39.6	1.20
58B	PMMA–PS–PMMA	0.50	110 ± 5	
58H	Precursor PS	1.00	55.8	1.38

Table II
Characteristics of Solvents

	PS	PMMA	ν, mL g^{-1} (436 nm, 30 °C) PS	PMMA
Toluene	Good	Good	0.113	0.004
p-Cymene	Good	Nonsolvent	0.121	0.011

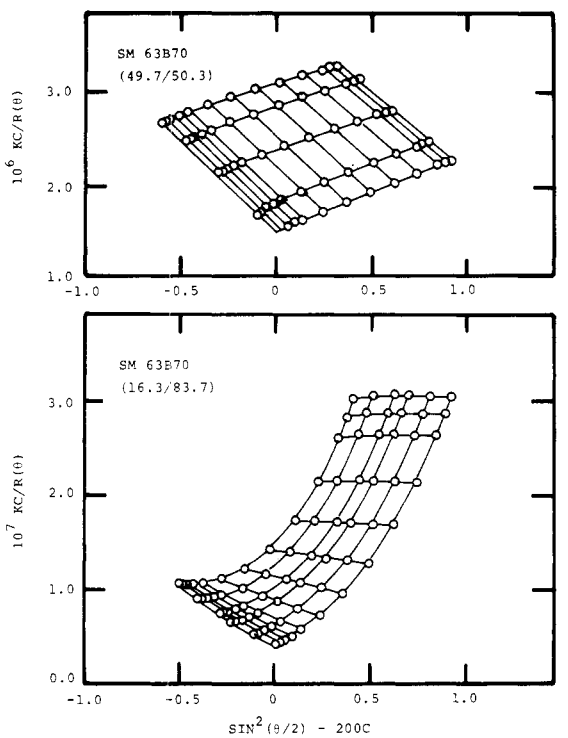

Figure 1. Typical Zimm plots for SM-diblock copolymer 63B70 in 49.7/50.3 (above) and 16.3/83.7 (below) TOL/pCY mixtures (by wt %) at 30.0 °C.

Results

Apparent Molecular Weights, Radii of Gyration, and Second Virial Coefficients. Figures 1 and 2 respectively show typical Zimm plots for the SM-diblock sample 63B70 and for the MSM-triblock sample 58B in TOL/pCY mixture. Each figure includes two cases: The one is just on the verge of the micelle formation, while in the other the micelle formation is evident, as judged from exceedingly large apparent molecular weight value M_{app} in comparison with that of the former. However, the shape of the Zimm plots in the micelle-forming solvents is quite different between those of the diblock and of the triblock samples, suggesting the difference in the micelle morphology. In certain cases of diblock copolymer solutions of micelle-forming compositions, the angular dependence of $Kc/R(\theta,c)$ plots showed considerable curvature (cf., Figure 1 below). Here K is the light-scattering constant and $R(\theta,c)$ is the Rayleigh ratio at a scattering angle θ and concentration

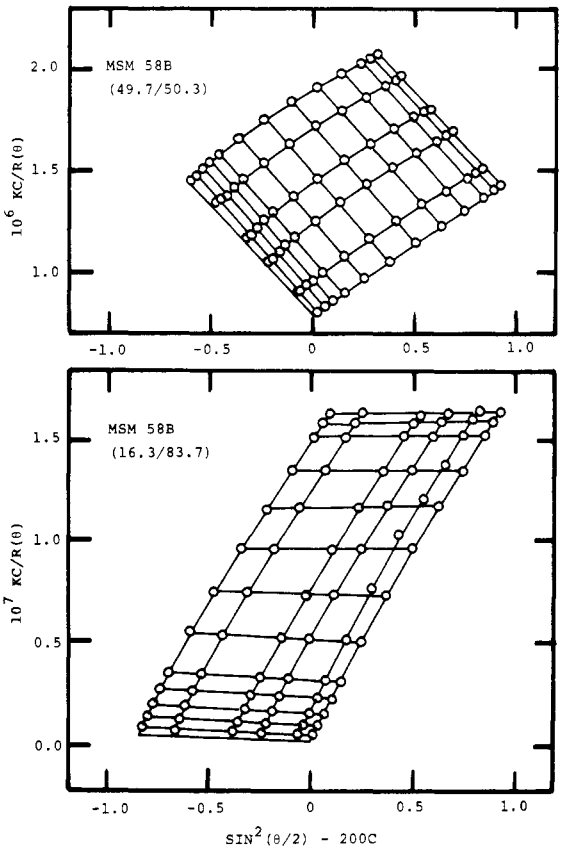

Figure 2. Typical Zimm plots for MSM-triblock copolymer 58B in 49.7/50.3 (above) and 16.3/83.7 (below) TOL/pCY mixtures (by wt %) at 30.0 °C.

c.[14] Therefore it was difficult to determine the value of the apparent mean-square radius of gyration $\langle s^2\rangle_{app}$ from $Kc/R(\theta,0)$ vs. $\sin^2(\theta/2)$ plot. To avoid this difficulty we plotted $\ln[Kc/R(\theta,0)]$, which showed better linearity in the range of small $\sin^2(\theta/2)$.

Table III summarizes the values of M_{app}, $\langle s^2\rangle_{app}^{1/2}$, and the apparent second virial coefficient A_2 for the SM- and MSM-block copolymers and their precursor PS solutions. Figure 3 shows the variation of M_{app}, A_2, and $\langle s^2\rangle_{app}^{1/2}$ with pCY content. As judged from intrinsic viscosity $[\eta]$ data, the θ composition (at 30 °C) of TOL/pCY mixture for PMMA is about 48 wt % pCY content.[3] In all the cases the M_{app} value begins to increase at a pCY centent somewhat larger than this value, and finally it reaches to about as large as 10^8 where macroscopic phase separation is about to take place. For the three SM 63B-series samples, these critical pCY contents are higher for those having shorter PMMA blocks.

The variation of A_2 on the solvent composition is similar to the results of Kurata et al.[8] It becomes slightly negative upon the incipient micelle formation, and then nearly zero (positive) value until the macroscopic phase separation takes place.

The variation of $\langle s^2\rangle_{app}^{1/2}$ is interesting especially for the SM 63B-series samples: In the molecularly dispersed region of low pCY content, the $\langle s^2\rangle_{app}^{1/2}$ value stays nearly constant equal to that of the precursor PS 63H; as soon as the micelle formation begins, it becomes about twice the value of a single block-copolymer molecule, and again it increases steeply as the pCY content is more and more increased. Namely they appear to show two-step variation in the $\langle s^2\rangle_{app}^{1/2}$ value, as opposed to the M_{app} value which increases steadily after the micelle formation. On the other hand the $\langle s^2\rangle_{app}^{1/2}$ value of the MSM-58B sample shows a much simpler dependence on the solvent composition. We should note that the results of

Table III
Summary of Light-Scattering Results on Polystyrene–Poly(methyl methacrylate) Block Copolymers in Toluene and *p*-Cymene Mixture at 30 °C

Code	Solvent composition, wt % toluene	μ_A	$10^{-6}M_{app}$	$\langle s^2\rangle_{app}^{1/2}$, Å	10^5A_2, g/mL
63B30	100	0.899	1.70	336	11.7
	78.2	0.868	2.14	356	10.4
	62.5	0.846	2.14	367	7.60
	49.7	0.831	2.09	336	3.86
	39.6	0.819	158	842	0.111
	30.1	0.808	334	1443	0.0393
63B50	100	0.965	0.838	270	26.8
	49.7	0.938	0.813	281	13.9
	39.7	0.932	5.08	664	−0.369
	30.1	0.927	26.4	685	0.669
	16.3	0.921	93.7	1250	0.295
63B70	100	0.984	0.631	253	35.5
	49.7	0.935	0.613	296	20.3
	40.3	0.933	0.619	319	17.2
	30.1	0.927	4.41	569	−2.20
	16.3	0.921	24.0	659	1.32
	0	0.914	206	2413	0.147
63H	100		0.392	252	47.0
	49.7		0.371	239	35.9
	0		0.323	224	26.5
58B	100	0.966	1.13	389	12.2
	73.4	0.951	1.23	385	16.1
	49.7	0.940	1.18	365	11.3
	40.3	0.936	2.31	795	10.3
	30.3	0.931	46.3	1095	−0.0257
	16.3	0.924	1290	6728	0.0381
58H	100		0.558	337	44.0
	49.7		0.550	320	34.0
	0		0.463	303	23.0

Kurata et al.[8] on a PS–PMMA diblock sample in TOL/FAL mixture showed a much complicated dependence of the $\langle s^2\rangle_{app}^{1/2}$ on the solvent composition particularly in the micelle-forming region.

Particle-Scattering Function. Extrapolating the Rayleigh ratio $R(\theta,c)$ to zero concentration, we can determine the particle-scattering function $P(\theta)$. If we employ an angular variable $X_{app} = \langle s^2\rangle_{app}\omega^2$ with $\omega = (4\pi/\lambda)\sin(\theta/2)$ (λ is the wavelength of light in the medium), the functions $P(\theta)$ or $P^{-1}(\theta)$ vs. X_{app} are dependent solely on the shape of a scattering particle, a molecule or a micelle whatever it is.[15,16] Figures 4 through 7 show plots of the reciprocal particle scattering function $P^{-1}(\theta)$ vs. X_{app} for the SM-diblock and MSM-triblock copolymers in TOL/pCY mixtures of the micelle-forming compositions.

For the SM-diblock copolymers we observe two distinctly different types of the P^{-1} vs. X_{app} plots: one type appears in the range of intermediate pCY content, and consists of a relatively small number (<100) of molecules, and the other type appears in the range of higher pCY content, and consists of a larger number (>100) of molecules. The P^{-1} vs. X_{app} plot of the former shows a considerable curvature, resembling that of a previously defined star-shape micelle,[4] i.e., a micelle consisting of a spherical (nearly invisible) PMMA core with (visible) PS arms stretching out of it. On the other hand, the plot of the latter resembles that of a more fully extended chain or a long thin rod, i.e., the P^{-1} increases with X_{app} more slowly than that of a Gaussian chain. These results correspond to the two-step variation of $\langle s^2\rangle_{app}^{1/2}$ with pCY content.

On the other hand, the MSM-triblock copolymer system in the micelle-forming region exhibits in the Zimm plots nearly rectilinear scattering envelopes (cf., Figure 2 below). The P^{-1} vs. X_{app} plots are slowly increasing functions of X_{app}, regardless of the pCY content or the micelle size, as seen in Figure 7.

Theoretical

Analysis of Spherical Micelle Morphology. In the behavior of the SM-diblock copolymers, particularly noteworthy are the two-step variation of $\langle s^2\rangle_{app}^{1/2}$ and the corresponding variation of the shape of the P^{-1} vs. X_{app} plots. These results suggest the formation of a micelle similar to the previously defined star-shape micelle[4] in the intermediate range of the pCY content, i.e., in the first stage of the two-step variation. Therefore we will explore this possibility a little further.[17,18] For this purpose we consider a "spherical-micelle" model.[18] We assume that f AB-diblock copolymer molecules, each consisting of N_A A segments and N_B B segments, aggregate to form a micelle. The B blocks form the spherical core and the A blocks the fringe of the micelle. The AB junction of a block copolymer chain is assumed on a spherical surface of radius r_0. The A chain obeys the random-flight statistics and is fully excluded from a hard core of radius a ($\leq r_0$). The B segments, on the other hand, are assumed to be uniformly distributed within the sphere, and then the shelllike region between a and r_0 constitutes an A–B intermixing phase. The previously defined "star-shape" model[4] is apparently a special case of $a = 0$ of the present model. The above assumption on the distribution of the B segments is apparently too crude. However, here we mainly consider a case where B blocks are nearly invisible because of isorefractive solvents. Hence the detail of the B-segment distribution would not affect the final results too seriously.

Overall Radial-Density Distribution. To derive the particle-scattering function for this model, first we have to know the radial-density distribution of the A segments of the model. Since the details were given in our previous article,[18] here we only give a brief summary. We consider a random-flight chain with $n + 1$ segments, numbered from 0 to n ($=N_A$), each of the same length b ($=b_A$). The first (0th) seg-

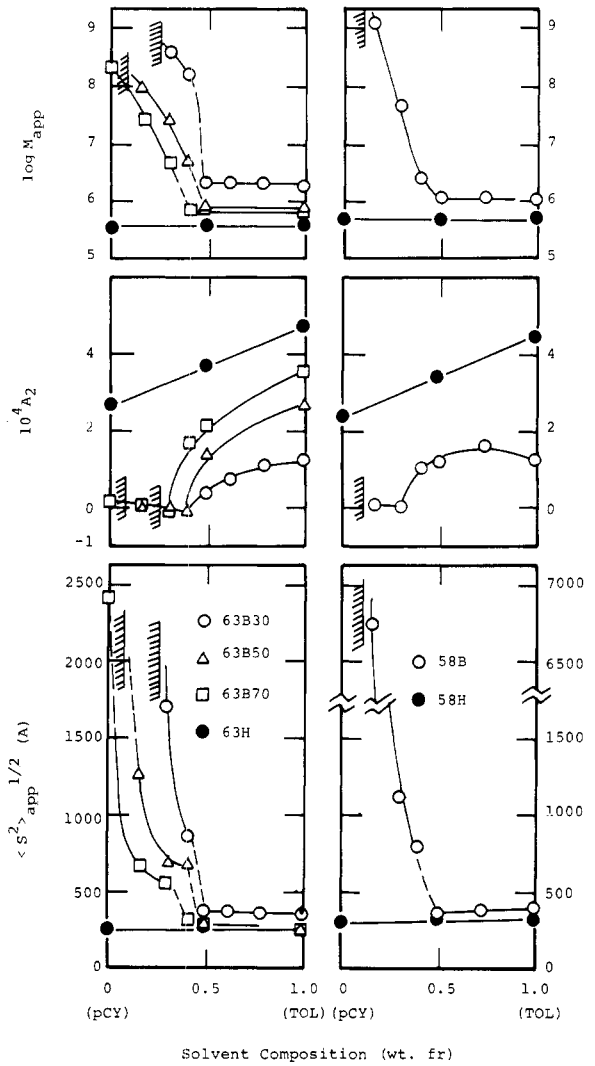

Figure 3. Plots of M_{app}, A_2, and $\langle s^2 \rangle_{app}^{1/2}$ vs. solvent composition for three SM 63B samples (left) and a MSM 58B sample (right) in a TOL/pCY mixture at 30.0 °C.

ment anchors at a point on the spherical surface of radius r_0. Since the distribution function $f_n(\mathbf{r}_n)$ of the end vector $\mathbf{r}_n$ is spherically symmetrical, a function $P_n = r_n f_n$ with $r_n = |\mathbf{r}_n|$ obeys a one-dimensional diffusion equation of the form

$$\partial p_n(r_n)/\partial n = (b^2/6)[\partial^2 p_n(r_n)/\partial r_n{}^2] \qquad (1)$$

The equation is to be solved under the conditions that the 0th segment is fixed at r_0 and all other segments are found in the region where $r > a$. In other words, the problem reduces to the one for a random-flight chain with one end bound at a point near an impermeable planar surface.[17] Following the procedure employed in such calculations, we obtain the probability density $p_n(r_i/r_0|a)$ of finding an ith segment at r_i under such restrictions. Then, with the normalization

$$\int_0^\infty 4\pi r_i{}^2 p_n(r_i/r_0|a)\, dr_i = 1$$

we have the normalized overall radial-density distribution $\rho_n(r/r_0|a)$ as

$$\rho_n(r/r_0|a) = (n+1)^{-1} \sum_{i=0}^{n} p_n(r_i/r_0|a), \quad r_i = r \qquad (2)$$

Introducing the expression for $p_n(r_i/r_0|a)$ into eq 2, converting the summation to an integral, and carrying out the integration by the Laplace folding operation, we finally have the following result[18]

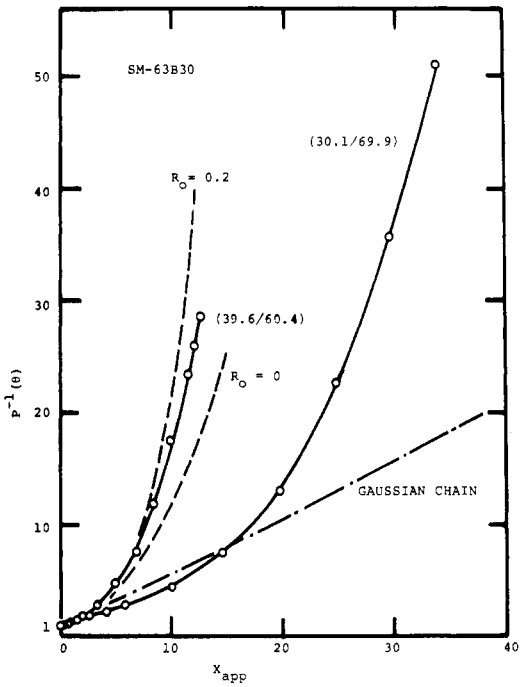

Figure 4. Reciprocal $P(\theta)$ vs. $X_{app} = \omega^2\langle s^2 \rangle_{app}$ plots for SM 63B30 sample at 30.0 °C in a TOL/pCY mixture with varying composition as indicated. Dashed curves are theoretical ones for some simple models.

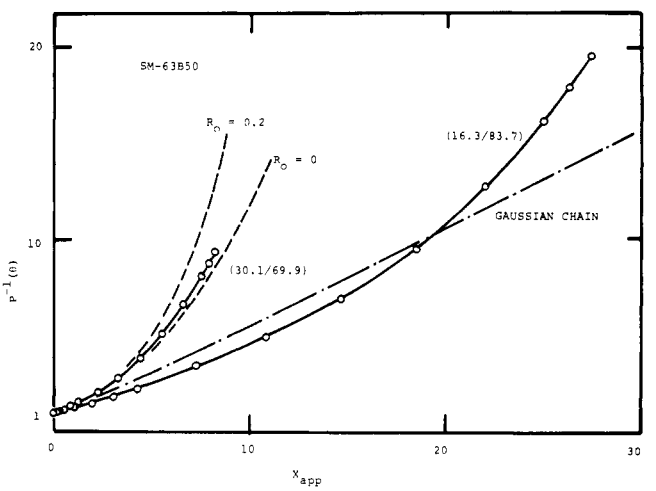

Figure 5. Reciprocal $P(\theta)$ vs. X_{app} plots for the SM 63B50 sample (cf. Figure 4).

$$\rho_{N_A}(r/r_0|a) \times (4\pi r^2) = 2(\beta/\pi)^{1/2}[R_0 - A + A\,\mathrm{erf}(R_0 - A)]^{-1} \times \{R[\exp(-h_1{}^2) - \exp(-h_2{}^2) - \pi^{1/2}h_1(1 - \mathrm{erf}(h_1)) + \pi^{1/2}h_2(1 - \mathrm{erf}(h_2))] + A[-\exp(-h_3{}^2) + \exp(-h_4{}^2) + \pi^{1/2}h_3(1 - \mathrm{erf}(h_3)) - \pi^{1/2}h_4(1 - \mathrm{erf}(h_4))]\} \qquad (3)$$

with

$$h_1 = |R - R_0|, \quad h_2 = R + R_0 - 2A \qquad (4a, b)$$

$$h_3 = h_1 + R - A, \quad h_4 = h_2 + R - A \qquad (4c, d)$$

Here the reduced lengths are defined as $R_0 = \beta^{1/2}r_0$, $A = \beta^{1/2}a$, $R = \beta^{1/2}r$, etc., with $\beta = 3/(2N_A b_A{}^2)$. For two extreme cases of $r_0 = a$ (or $R_0 = A$) and $a = 0$ (or $A = 0$), we respectively have

$$\rho_{N_A}(r/r_0|a = r_0) \times (4\pi r^2) = 4\beta^{1/2}(1 + 2A/\pi^{1/2})^{-1}\{R[1 - \mathrm{erf}(R - A)] - A[1 - \mathrm{erf}(2R - 2A)]\} \qquad (5)$$

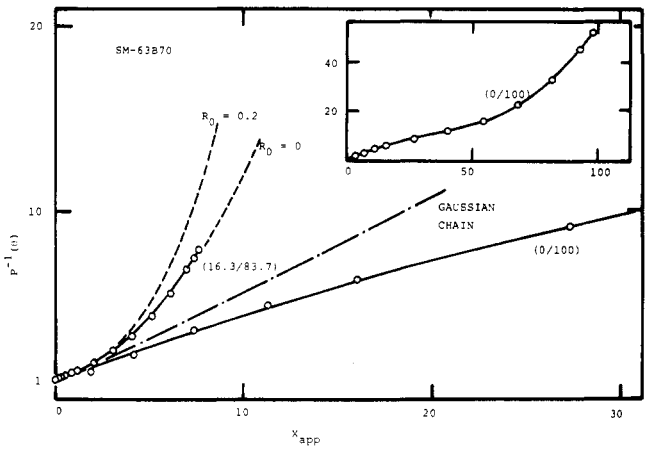

Figure 6. Reciprocal $P(\theta)$ vs. X_{app} plots for the SM 63B70 sample (cf. Figure 4).

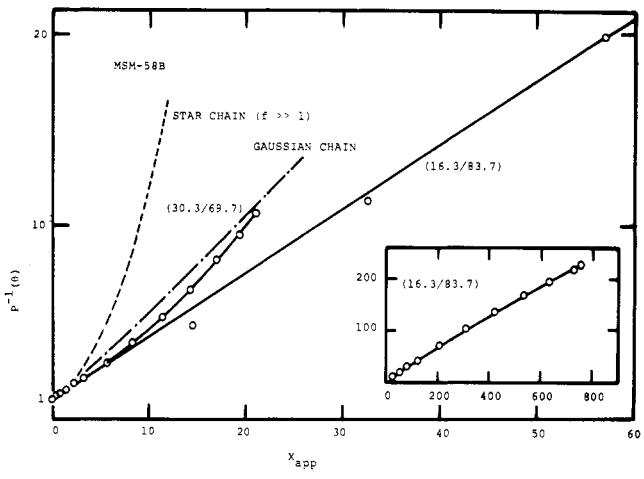

Figure 7. Reciprocal $P(\theta)$ vs. X_{app} plots for the MSM 58B sample (cf. Figure 4).

and

$$\rho_{N_A}(r/r_0|0) \times (4\pi r^2) = 2(\beta/\pi)^{1/2}(R/R_0) \times [\exp(-h_1^2) - \exp(-h_2^2) - \pi^{1/2}h_1(1 - \mathrm{erf}(h_1)) + \pi^{1/2}h_2(1 - \mathrm{erf}(h_2))] \quad (6)$$

The former is a case of complete segreation, i.e., of no intermixing phase, while the latter is a case of freely intermixing which is equivalent to the previous "star-shape" model.[4]

Particle-Scattering Function. The particle-scattering function of an AB binary copolymer is generally given as[6]

$$P(\theta) = \mu_A^2 P_A(\theta) + \mu_B^2 P_B(\theta) + 2\mu_A\mu_B P_{AB}(\theta) \quad (7)$$

$$\mu_A = 1 - \mu_B = x\nu_A/(x\nu_A + y\nu_B) \quad (8)$$

where $P_K(\theta)$ and $P_{AB}(\theta)$ represent the interferences between the same and different segments, respectively; $x = 1 - y$ is the weight fraction of A segments; and ν_K is the specific refractive index increment of K homopolymer (K = A or B). For the micelle model of f arms, $P_A(\theta)$ may be conveniently split into two terms, $P_{A,1}$ and $P_{A,2}$, which represent the intra- and the interchain contribution, respectively:

$$P_A(\theta) = f^{-1}P_{A,1} + (1 - f^{-1})P_{A,2} \quad (9)$$

The intrachain term $P_{A,1}$ may be approximated by the Debye function for a random-flight chain[15]

$$P_{A,1} \simeq (2/Y_A)^2[\exp(-Y_A) - 1 + Y_A] \quad (10)$$

$$Y_A = \omega^2/4\beta = \omega^2(N_A b_A^2/6) \quad (11)$$

The interchain term may be calculated from eq 4 as

$$P_{A,2}^{1/2} = \int_a^\infty 4\pi r^2 \rho_{N_A}(r/r_0|a) \sin(\omega r)/(\omega r)\, dr \quad (12)$$

The integration cannot be carried out analytically except for an extreme case of $a = 0$,[18] where we have

$$P_{A,2}^{1/2} = \sin U_B[1 - \exp(-Y_A)]/(U_B Y_A) \quad (13)$$

$$U_B = r_0\omega \quad (14)$$

For other cases we carried out the integration by a numerical calculation using a Monte Carlo method.[17-19]

Since we assumed a uniform density for the B sphere of radius r_0, we have

$$P_B^{1/2}(\theta) = (3/U_B^3)(\sin U_B - U_B \cos U_B) \quad (15)$$

For $P_{AB}(\theta)$, we have

$$P_{AB}(\theta) = P_{A,2}^{1/2}(\theta)P_B^{1/2}(\theta) \quad (16)$$

From eq 12, 15, and 16 with adequate choice of μ_A and μ_B, we can calculate the $P(\theta)$ function for the present micelle model.

Apparent Radius of Gyration. Light-scattering apparent mean-square radius of gyration $\langle s^2\rangle_{app}$ of a binary copolymer is given by[6]

$$\langle s^2\rangle_{app} = \mu_A^2\langle s^2\rangle_A + \mu_B^2\langle s^2\rangle_B + 2\mu_A\mu_B\langle s^2\rangle_{AB} \quad (17)$$

Corresponding to the $P(\theta)$ function, $\langle s^2\rangle_A$, $\langle s^2\rangle_B$, and $\langle s^2\rangle_{AB}$ terms are given for the present model, respectively, as

$$\langle s^2\rangle_A = f^{-1}\langle s^2\rangle_{A,1} + (1 - f^{-1})\langle s^2\rangle_{A,2} \quad (18)$$

$$\langle s^2\rangle_{A,1} \simeq 1/4\beta = N_A b_A^2/6 \quad (19)$$

$$\langle s^2\rangle_{A,2} = \int_a^\infty 4\pi r^2 \rho_{N_A}(r/r_0|a)\, dr \quad (20)$$

$$\langle s^2\rangle_B = (3/5)r_0^2 \quad (21)$$

$$\langle s^2\rangle_{AB} = (1/2)(\langle s^2\rangle_{A,2} + \langle s^2\rangle_B) \quad (22)$$

Here the $\langle s^2\rangle_{A,2}$ term can be calculated analytically for the two extreme cases: one is for $r_0 = a$

$$\beta\langle s^2\rangle_{A,2} = 3/4 + R_0^2 + (7/3\pi^{1/2})R_0[1 + (9/14)\pi^{1/2}R_0]/(1 + 2\pi^{-1/2}R_0) \quad (23)$$

and the other is for $a = 0$

$$\beta\langle s^2\rangle_{A,2} = 3/4 + R_0^2 \quad (24)$$

For the general case, eq 20 was again calculated numerically by a Monte Carlo method.[18]

Behavior of the "Spherical Micelle" Model. From eq 7 through 24, we can calculate theoretical $P^{-1}(\theta)$ vs. X_{app} relations for the model, using R_0 and A/R_0 as adjustable parameters. First we consider a case where B blocks are completely invisible, i.e., $\mu_B = 0$. In the calculation we further assume that the number of arms f be sufficiently large so that $f^{-1} \ll 1$, $\langle s^2\rangle_{app} \simeq \langle s^2\rangle_{A,2}$, and $P(\theta) \simeq P_{A,2}$. Figure 8 shows plots of $P^{-1}(\theta)$ vs. X_{app}, which are equivalent to $P_{A,2}^{-1}$ vs. $X_{A,2}$, for several values of R_0 with $A/R_0 = 1$. For $R_0 = 0$, the model reduces to a star molecule with a large number of arms. The P^{-1} increases with increasing X_{app} much more rapidly than that of a random-flight chain. We see that the larger the radius of the invisible B sphere the larger the curvature of the curve at small values of X_{app}, i.e., at low angles. This severe curvature suggests that the extrapolation of experimental $Kc/R(\theta,0)$ vs. $\sin^2(\theta/2)$ plots to zero angle should be very difficult. However, if we plot $\ln P^{-1}(\theta)$ against X_{app}, we observe a better linearity at low angles. This is the reason why we employed $\ln Kc/R(\theta,0)$ vs. $\sin^2(\theta/2)$ plots to estimate $\langle s^2\rangle_{app}$ values in the previous section.

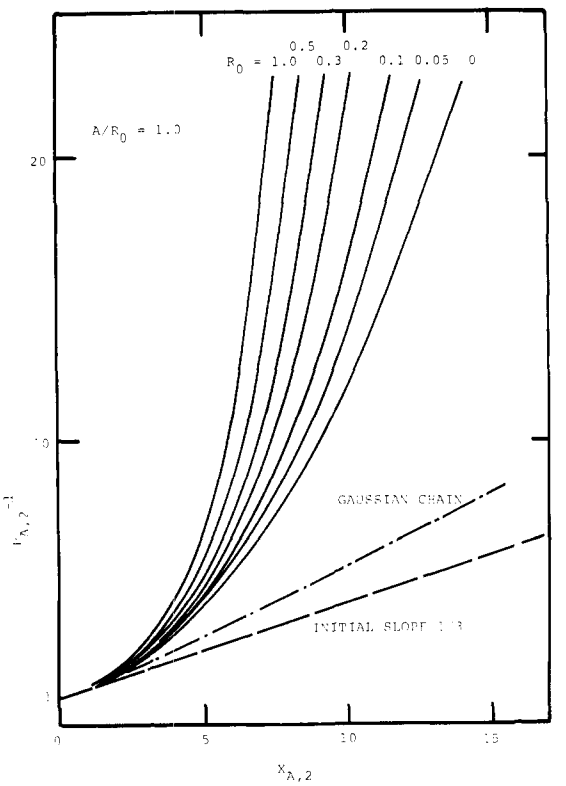

Figure 8. Theoretical $P^{-1}(\theta)$ vs. X_{app} plots for the "spherical micelle" model with complete segregation approximation (A/R_0 = 1.0) and varying R_0 as indicated. The core was assumed invisible (μ_B = 0).

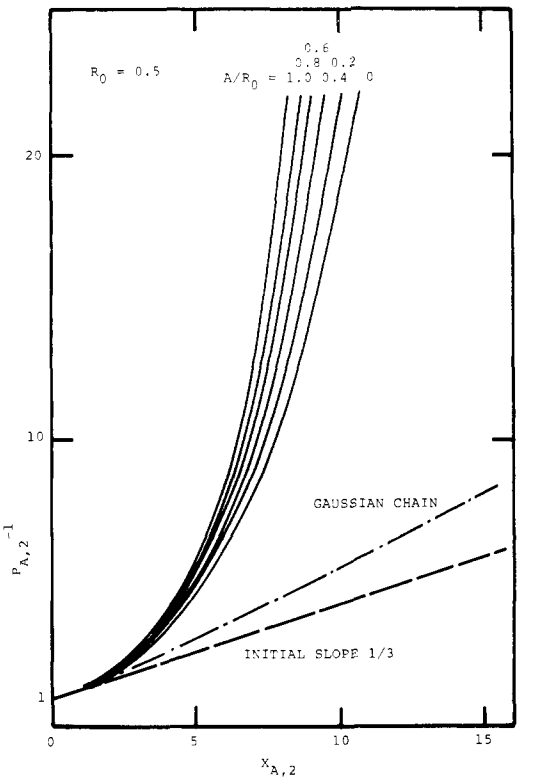

Figure 9. Theoretical $P^{-1}(\theta)$ vs. X_{app} plots for the "spherical micelle" model with a fixed R_0 (=0.50) and varying thickness of the intermixing phases A/R_0 as indicated. The core was assumed invisible (μ_B = 0).

Figure 9 shows similar plots for a given R_0 (=0.5) and varying A/R_0 values. As the thickness of the intermixing phase increases, the $P^{-1}(\theta)$ vs. X_{app} curve shifts slightly toward that of a random-flight chain, although the shift is not very large. The feature implies that the shape of the $P(\theta)$ function is determined essentially by the size of the central invisible core relative to the length of the visible fringe.

As to the effect of the small visibility of PMMA blocks, we expect the effect to be rather small in this model, because the visible PS blocks constitute the more expanded fringe part, from which the dominant contribution to the scattered-light intensity arises, and the contribution from the (nearly invisible) core should be trivial. In this connection, of interest is the behavior of micelles reported by Kurata et al.,[8] a PS–PMMA diblock copolymer in TOL/FAL mixture, in which visible PS (=B) blocks constitute the core and slightly visible PMMA (=A) blocks in the fringe part of the micelle. For such micelles the density profile of PS blocks within the core should be more important. However, here we only wish to demonstrate the contribution from slightly visible but more expanded PMMA blocks, still assuming a uniform density of the PS core.

The correction factors may be readily calculated from eqs 17 through 22 with the numerical values of $\langle s^2\rangle_{A,2}$. For the micelle model with a large number of arms, i.e., $f \gg 1$, the $\langle s^2\rangle_{app}$ equation assumes a simple form:

$$\langle s^2\rangle_{app} = \mu_A\langle s^2\rangle_{A,2} + \mu_B\langle s^2\rangle_B \qquad (25)$$

In Table IV the corrections for $\langle s^2\rangle_{app}$ due to the nearly invisible blocks are summarized for such a simple case of $f \gg 1$ and A/R_0 = 1.0. The table contrasts two cases, i.e., the one with the nearly invisible fringe and the other with the nearly invisible core. For the former case the correction is exceedingly large especially for that with a small core and extended fringes: The $\langle s^2\rangle_{app}$ is always much larger than the true $\langle s^2\rangle_B$ values. On the other hand, for the latter case the $\langle s^2\rangle_{app}$ is always smaller than the true $\langle s^2\rangle_A$ value and much less sensitive to the micelle geometry, i.e., to the value of R_0.

Table IV
Correction Factors to Apparent Mean Square Radii from Slightly Visible Segments of the "Spherical Micelle" Model

	Micelles with slightly visible fringes $\langle s^2\rangle_{app}/\langle s^2\rangle_B$		Micelles with slightly visible core $\langle s^2\rangle_{app}/\langle s^2\rangle_A$	
R_0	μ_A = 0.05	μ_A = 0.10	μ_B = 0.05	μ_B = 0.10
0.2	3.145	5.290	0.951	0.902
0.4	1.699	2.398	0.953	0.907
0.6	1.390	1.781	0.956	0.911
0.8	1.269	1.537	0.958	0.916
1.0	1.206	1.412	0.960	0.920
1.2	1.169	1.337	0.961	0.923

Discussion

From the data shown in Table III and Figure 3, we see that the behavior of the SM-diblock copolymers in the TOL/pCY mixture may be classified into three categories: the one is the region of low pCY content where the block copolymer molecules are presumably in the state of moecular dispersion; the second is the region of intermediate pCY content where spherical or nearly spherical shape micelles are presumably present; and the third is the region of high pCY content where micelles of large size and unusual morphology are present. On the other hand, the behavior of the MSM triblock copolymer appears to be classified into only two categories: one is the region of low pCY content where isolated molecules are present; and the other is the micelle-forming region of intermediate to high pCY content.

As to the behavior in the low pCY content region, the behavior of both SM-diblock and MSM-triblock copolymers completely conforms to our previous conclusions.[9,10,12] For

the diblock copolymers the slight descrepancy between their $\langle s^2\rangle_{app}$ values and that of the precursor PS chains may be ascribed to the effect of the small visibility of PMMA blocks in this solvent system.[9,12] For the MSM-triblock copolymer, the $\langle s^2\rangle_A$ value as corrected for the slight visibility of PMMA side blocks is still about 15% larger than that of the precursor PS chains.[10]

"Spherical Micelle" Model for SM-Diblock Copolymers. On the other hand, the behavior of the SM-diblock copolymers in the intermediate pCY content appears to comply with the behavior of the "spherical micelle" model. To carry out an analysis based on the model, we first need to determine the model parameters. The (average) number of molecules f_n involved in a micelle may be defined as the ratio of the number average molecular weights of the micelles M_n* and the individual block copolymer molecules M_n. The micelles may be regarded as a kind of star-shape block copolymer with a large number of arms. Then according to our previous analysis[20,21] the M_{app}* and M_n* may be related as

$$M_{app}^* = (1 + \mu_A^2 Y_A^* + \mu_B^2 Y_B^*)M_n^* \qquad (26)$$

with $Y_K^* = Y_K f^{-1} = \{(M_w^K/M_n^K) - 1\}f^{-1}$ where M_w^K and M_n^K (K = A or B) are the weight and number-average molecular weights of K precursors. For the micelles we may assume that f is sufficiently large and then $M_{app}^* = M_n^*$. This is because the molecular weight and compositional heterogeneities of the micelles should be smoothed out to a large extent upon formation of multimolecular micelles. For the original molecules, we may assume $f = 1$. Therefore for f_n we have

$$f_n \simeq M_{app}^*(1 + \mu_A^2 Y_A + \mu_B^2 Y_B)/M_{app} \qquad (27)$$

with M_{app} being the value for the original block copolymer molecules as determined from the data in nonmicelle-forming solvent, e.g., toluene. (Measurements in toluene have an additional advantage for the present system, because here $\mu_B \simeq 0$ and the value Y_A is determined from the precursor PS data such as listed in Table I.)

In addition to this, the model involves three parameters R_0, A, and β, while the data available are essentially two: $\langle s^2\rangle_{app}$ and $P^{-1}(\theta)$ vs. X_{app} curve. Therefore there is no unequivocal way of determining these parameters simultaneously. The shape of the theoretical $P^{-1}(\theta)$ vs. X_{app} plot is determined by the parameters R_0 and A/R_0. Then they may be chosen so as to achieve a fitting between the theoretical and experimental curves. However, several different combinations of R_0 and A/R_0 yield a nearly identical $P(\theta)$ function so far as the values of X_{app} are within the range of practical interest. On the other hand the $\langle s^2\rangle_{app}$ value involves three parameters, β, R_0, and A/R_0, in such a way that $\beta\langle s^2\rangle_{app}$ is a function of R_0 and A/R_0. Here again several different combinations of R_0 and A/R_0, which give an identical $P^{-1}(\theta)$ vs. X_{app} plot, also give a nearly identical value of $\beta\langle s^2\rangle_{app}$. Therefore we cannot uniquely determine the values of R_0 and A/R_0.

A possible route to circumvent this situation is to assume an adequate value for one of the parameters and to determine the other from experiments. As we have seen in the preceding section, the theoretical curve is less sensitive to the choice of A/R_0. Hence we assume two cases: a complete segregation, $A/R_0 = 1.0$, and a free intermixing, $A/R_0 = 0$. We compare the experimental data with the theoretical curves, such as shown in Figure 10, to assign the value of R_0. In such an analysis we have adequately taken into account the effect of the slight visibility of the PMMA core by eq 7 through 16. Assigning the values of R_0 and A/R_0 by such a curve fitting, we can determine the theoretical $\beta\langle s^2\rangle_{app}$, which is then combined with the experimental $\langle s^2\rangle_{app}$ to give the value of $\beta = (4\langle s^2\rangle_{A,1})^{-1}$. From these values we can further estimate various model

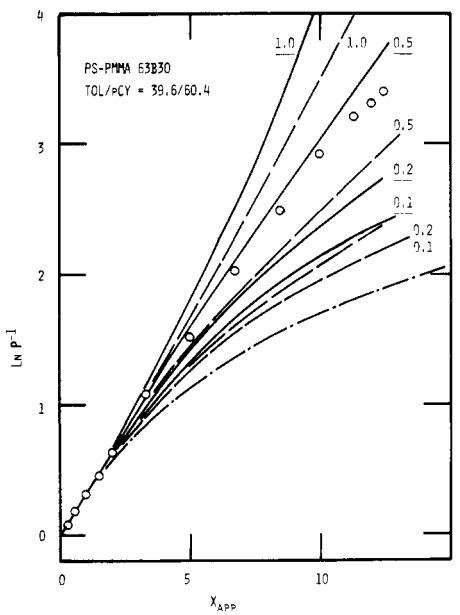

Figure 10. Comparison of theoretical and experimental ln $P^{-1}(\theta)$ vs. X_{app} plots for the SM 63B30 sample in a TOL/pCY (39.6/60.4) mixture at 30.0 °C. Solid curves are for complete segregation models, dashed curves for freely intermixing models, and a chain curve for a Gaussian chain. In the theoretical plots, slight visibility of the core was taken into account assuming $\mu_B = 0.181$ by eq 7 through 25.

parameters such as the core radius $r_0 = \beta^{-1/2}R_0$ and the PMMA density in the core $\rho_B = x_B M_{app}^*/N_0(4\pi/3)r_0^3$ with N_0 being the Avogadro number.

Here we should note an interesting implication of the parameter β. If there is no excluded volume interactions among the fringe chains and between the core and the fringe chains, the parameter β^{-1} ($=2N_A b_A^2/3$) should be equal to $4\langle s^2\rangle_{A,H}$, where $\langle s^2\rangle_{A,H}$ is the mean-square radius of the precursor A (=PS) chains. Then the ratio $\alpha_1^2 = (4\beta\langle s^2\rangle_{A,H})^{-1}$ represents the expansion of the fringe chains in the radial direction due to such excluded volume interactions.

All these parameter values are summarized in Table V, where the two cases are compared. Examining these results we notice the following few points. First of all, regardless of the models employed the values of α_1 are nearly the same and assume a considerably larger value in each system. For an isolated chain of AB-diblock or BAB-triblock copolymers, we found that the B chains are only slightly (perhaps less than 10%) expanded in the radial direction.[9,10] However, in the micelles the fringe PS chains are considerably extended in the radial direction presumably due to the interchain interactions.

Second we notice that the core radius of the micelles is larger for those having larger PMMA blocks. According to Meier[22] a typical domain size D, e.g., the radius of a spherical domain, is given as

$$D = k\alpha(\sigma l^2)_0^{1/2} \qquad (28)$$

where σ is the number of statistical segments of length l; the subscript 0 denotes the unperturbed state and α is a perturbation parameter, i.e., the ratio of perturbed to unperturbed chain dimensions, $\alpha^2 = (\sigma l^2)/(\sigma l^2)_0$, and k is a numerical parameter that depends on domain shape and molecular architecture and $k = 1.33$ for spherical domain of AB-diblock copolymers. Interestingly eq 28 does not involve the number of molecules f_n in a domain. This would explain the fact that in the first stage of the micelle formation the $\langle s^2\rangle_{app}$ of the SM-diblock copolymers stays nearly the same, while the M_{app} of the same system rapidly increases with increasing pCY content. In other words the increase in f_n does not alter the

Table V
Summary of the "Spherical Micelle" Model Parameters for Complete Segregation ($A = R_0$) and Freely Intermixing ($A = 0$) Cases of PS–PMMA-Diblock Copolymers in the TOL/pCY Mixture at 30 °C

Code	63B30	63B50	63B70
(TOL/pCY)	(39.6/60.4)	(30.1/69.9)	(16.3/83.7)
f_n	108	37.0	45.1
Complete Segregation Model ($A = R_0$)			
R_0	0.42	0.18	0.10
r_0, Å	320	130	72
ρ_B, g mL^{-1}	1.45	2.43	7.90
α_1	1.62	1.52	1.56
Freely Intermixing Model ($A = 0$)			
R_0	0.70	0.45	0.35
r_0, Å	551	321	249
ρ_B, g mL^{-1}	0.285	0.161	0.192
α_1	1.67	1.53	1.55

shape and size of the spherical micelles. Assuming $\alpha = 1$ in eq 28, we estimated the domain size D (in Å) of the micelles to be 908 for 63B30, 530 for 63B50 and 380 for 63B70. These values are about two to three times larger than those listed in Table V. This is because the PMMA blocks in the micelles are assuming a more compact conformation than the unperturbed conformation, since they are subjected to the solvent mixture which has the pCY content much higher than the corresponding θ composition.

Third we notice that the core radius estimated in Table V is considerably different depending on the approximations employed: The complete segregation model naturally predicts a much smaller core than the freely mixing model does. If we estimate the PMMA density ρ_B in the core, we find that the core density for the former model is more than the bulk density. This is apparently too high. On the other hand, for the latter model the core density might be too low. Recent SAXS studies of Kawai et al.[23,24] on the domain boundary structure of polystyrene–polyisoprene diblock copolymer films suggest the presence of about 10% thickness intermixing phase even in the bulk block copolymer. Therefore for the solvent-swollen micelles in dilute solution such as of the present study, a considerable extent of intermixing must have been taking place. For example, if we assume a core density $\rho_B = 0.7$ g/mL for the three systems, we find the ratio of the intermixing phase thickness to the core radius (in A) as 50/370 for 63B30, 60/190 for 63B50, and 90/160 for 63B70. This much of intermixing seems to be quite reasonable. Presumably the core density in the block copolymer systems is equal to the concentration of the dense phase in a corresponding PMMA–TOL–pCY ternary system so long as the pure PMMA and solvent phase and the dilute solution phase exist (regardless of the existence of a PS and PMMA intermixing phase). Such a phase-separation study on PMMA–TOL–pCY ternary systems would provide an additional criterion for determining the micelle morphology.

Micelles of Other Morphologies. The light-scattering results suggest that increasing pCY content in a SM-diblock copolymer system results in the formation of micelles with entirely different morphology: The micelles should have a more extended shape rather than a spherical shape, as judged from the fact that the reciprocal $P(\theta)$ function of such micelles is a more slowly increasing function of X_{app} than that of a Gaussian chain at least in the range of small X_{app} (cf. Figures 4 through 6). Increase in pCY content in the system drives PMMA blocks to form more compact and much larger aggregates, which is counteracted by the presence of PS blocks. In view of Meier's arguments,[20] we would expect that the domain size cannot change unless the domain shape changes to one of the other morphologies. What happened was that as the number of participating molecules increases (while keeping the same core shape) and the core density has come to exceed the thermodynamically stable value (since the domain size changes only slightly as solvent becomes poorer), a change of the core shape must have taken place presumably by coalescing spherical cores to form a more extended ellipsoidal or cylindrical shape. A quantitative analysis of the morphology of such large micelles[25] remains to be solved.

On the other hand, the morphology of the MSM-triblock copolymer appears to differ from the spherical micelle in the intermediate and high pCY content regions (cf. Figure 7). This is not surprising, since each triblock molecule has two PMMA side blocks and successive aggregation of the PMMA blocks would end up with a network-like structure or a highly branched-type structure. Kajiwara, Burchard, and Gordon[26,27] developed a theory of Rayleigh scattering from such a highly branched structure and showed that the system should exhibit in Zimm plots rectilinear scattering envelopes. The Zimm plot of the MSM-58B system (cf. Figure 2) implies the existence of such a highly branched structure, although a quantitative comparison of the present data with their theory is difficult.

References and Notes

(1) (a) Osaka University; (b) Kyoto University.
(2) S. Krause, *J. Phys. Chem.*, **68**, 1948 (1964).
(3) T. Kotaka, T. Tanaka, and H. Inagaki, *Polym. J.*, **3**, 327 (1972).
(4) T. Tanaka, T. Kotaka, and H. Inagaki, *Polym. J.*, **3**, 338 (1972).
(5) M. Leng and H. Benoit, *J. Polym. Sci.*, **57**, 263 (1962).
(6) See also, H. Benoit and D. Frolich in "Light Scattering from Polymer Solutions", M. Huglin, Ed., Academic Press, London, 1972, Chapter 11.
(7) H. Utiyama, K. Takenaka, M. Mizumori, and M. Fukuda, *Macromolecules*, **7**, 28 (1974).
(8) H. Utiyama, K. Takenaka, M. Mizumori, M. Fukuda, Y. Tsunashima, and M. Kurata, *Macromolecules*, **7**, 515 (1974).
(9) T. Tanaka, T. Kotaka, and H. Inagaki, *Macromolecules*, **9**, 561 (1976).
(10) T. Tanaka, T. Kotaka, M. Hattori, K. Ban, and H. Inagaki, *Macromolecules*, in press.
(11) H. Ohnuma, T. Kotaka, and H. Inagaki, *Polymer*, **10**, 501 (1969).
(12) T. Tanaka, T. Kotaka, and H. Inagaki, *Macromolecules*, **7**, 311 (1974).
(13) M. Hattori, MS dissertation, Department of Polymer Chemistry, Kyoto University, 1976.
(14) See, for example, B. H. Zimm, *J. Chem. Phys.*, **16**, 1093, 1099 (1948).
(15) P. Debye, *J. Appl. Phys.*, **15**, 338 (1944); *J. Phys. Colloid Chem.*, **51**, 18 (1947).
(16) For block copolymers, an additional difficulty arises from the fact that the constituent blocks usually have different scattering powers.
(17) T. Tanaka, *Macromolecules*, **10**, 51 (1977).
(18) T. Tanaka, T. Kotaka, and H. Inagaki, *Bull. Inst. Chem. Res., Kyoto Univ.*, **55**, 150 (1977): detailed numerical data are available upon request.
(19) In the previous article (ref 4), the expression for this model is different due to the approximation employed then; the factor $\exp(-U_B^2/3)$ in eq 17 of ref 4 should be replaced by $(\sin U_B/U_B)^2$ to obtain the more rigorous expression given here.
(20) T. Kotaka, N. Donkai, and T. I. Min, *Bull. Inst. Chem. Res., Kyoto Univ.*, **52**, 332 (1974).
(21) T. Kotaka, *Bull. Inst. Chem. Res., Kyoto Univ.*, **55**, 135 (1977).
(22) D. J. Meier in "Block and Graft Copolymers", J. J. Burke and V. Weiss, Ed., Syracuse University Press, Syracuse, N.Y., 1973, Chapter 6.
(23) T. Hashimoto, K. Nagatoshi, A. Todo, H. Hasegawa, and H. Kawai, *Macromolecules*, **7**, 364 (1974).
(24) T. Hashimoto, A. Todo, H. Itoi, and H. Kawai, *Macromolecules*, **10**, 377 (1977).
(25) T. Kotaka, T. Tanaka, and H. Inagaki, unpublished.
(26) K. Kajiwara, W. Burchard, and M. Gordon, *Br. Polym. J.*, **2**, 110 (1970).
(27) W. Burchard, K. Kajiwara, M. Gordon, J. Kalal, and J. W. Kennedy, *Macromolecules*, **6**, 642 (1973).